Journal of Volcanology and Geothermal Research 358 (2018) 124–131

Contents lists available at ScienceDirect

Journal of Volcanology and Geothermal Research

journal homepage: www.elsevier.com/locate/jvolgeores

Volatile contents of primitive bubble-bearing melt inclusions from Klyuchevskoy volcano, Kamchatka: Comparison of volatile contents determined by mass-balance versus experimental homogenization

Moore Lowell R. [a,*], Mironov Nikita [b], Portnyagin Maxim [b,c], Gazel Esteban [d], Bodnar Robert J. [a]

[a] Department of Geosciences, Virginia Tech, Blacksburg, VA 24061, USA
[b] V.I. Vernadsky Institute of Geochemistry and Analytical Chemistry, Kosygin 19, 119991 Moscow, Russia
[c] GEOMAR Helmholtz Center for Ocean Research, Kiel, Wischhofstrasse 1-3, 24148 Kiel, Germany
[d] Department of Earth and Atmospheric Sciences, Cornell University, Ithaca, NY 14853-1504, USA

ARTICLE INFO

Article history:
Received 31 October 2017
Received in revised form 9 March 2018
Accepted 12 March 2018
Available online 13 March 2018

Keywords:
Melt inclusion
Raman
Volcanic degassing
Shrinkage bubble
Volatiles
Experimental rehydration

ABSTRACT

Primitive olivine-hosted melt inclusions provide information concerning the pre-eruptive volatile contents of silicate melts, but compositional changes associated with post-entrapment processes (PEP) sometimes complicate their interpretation. In particular, crystallization of the host phase along the wall of the melt inclusion and diffusion of H^+ through the host promote CO_2 and potentially S or other volatiles to exsolve from the melt into a separate fluid phase. Experimental rehomogenization and analysis of MI, or a combination of Raman spectroscopy, numerical modeling, and mass balance calculations are potentially effective methods to account for PEP and restore the original volatile contents of melt inclusions. In order to compare these different approaches, we studied melt inclusions from a suite of samples from Klyuchevskoy volcano (Kamchatka Arc) for which volatile compositions have been determined using experimental rehydration, Raman spectroscopy, and numerical modeling. The maximum CO_2 contents of melt inclusions are in agreement (~3600–4000 ppm), regardless of the method used to correct for CO_2 in the bubble, but significantly more uncertainty is observed using mass balance calculations. This uncertainty is largely due to the lack of precision associated with the petrographic method of determining bubble volumes and may also be related to the presence of daughter minerals at the glass-bubble interface.

1. Introduction

Information concerning the pre-eruptive volatile contents of magmas provides important constraints on local volcanic processes and global cycling of various elements in the Earth system. For example, the pre-eruptive concentrations of CO_2 and H_2O in the melt affect the depth and intensity of volcanic degassing and the explosivity of volcanic eruptions (Metrich and Wallace, 2008). Mantle temperatures can be estimated based on the H_2O concentration in the melt (Sobolev and Danyushevsky, 1994; Portnyagin et al., 2007; Gazel et al., 2012), and the CO_2 content of a melt may be related to the composition of the source lithology (e.g. anhydrous vs carbonated peridotite). The CO_2 concentrations of early-forming melts also have implications regarding the amount of CO_2 subducted into the mantle (e.g. Wallace, 2005), how deep carbon-bearing phases are subducted (Dasgupta, 2013), and how much subducted carbon eventually outgasses into the atmosphere (Burton et al., 2013). Much of our knowledge about magmatic volatile budgets comes from remote sensing and in situ sampling at active volcanoes (Burton et al., 2013). While these methods are effective for active volcanic systems, they cannot be applied to extinct or dormant volcanic systems. Furthermore, studies of diffuse degassing (e.g. Chiodini et al., 2004) suggest that volatile fluxes from a single point-source may significantly under-estimate the total volcanic degassing flux. As an alternative, melt inclusions preserve samples of pre-eruptive melt and provide a valuable tool for determining the volatile contents and degassing behavior of magmas (Roedder, 1979; Roedder, 1984).

Although melt inclusions can be a robust source of information, various post-entrapment processes (PEP) can modify the composition of the melt inclusions (e.g. glass, fluid) and complicate the interpretation of melt inclusion data to determine the volatile budget of the melt that was trapped in the inclusion. As a result, it is often difficult to determine whether compositional variations within a group of (presumably) coeval melt inclusions reflect local variations in melt chemistry during trapping or reflect processes that have occurred after the melt inclusion formed. For example, when a melt inclusion is trapped, post-entrapment crystallization (PEC) leads to depletion of elements that

* Corresponding author.
E-mail address: moorelr@vt.edu. (L.R. Moore).

https://doi.org/10.1016/j.jvolgeores.2018.03.007
0377-0273/

are compatible in the host mineral (Roedder, 1979; Danyushevsky et al., 2002). Furthermore, because the relative change in molar volume (or density) of the host mineral is less than that of the melt during cooling, the volume change associated with crystallization results in the formation of a "shrinkage bubble," depressurization within the inclusion, and degassing of volatile components (particularly CO_2) into the bubble (Roedder, 1979; Esposito et al., 2011; Moore et al., 2015; Aster et al., 2016). Additionally, it has also been shown that H_2O can be lost from olivine-hosted melt inclusions as the inclusion cools (Roedder, 1979; Sobolev and Danyushevsky, 1994) as a result of diffusion of H^+ across point defects in the host mineral (Mironov and Portnyagin, 2011; Gaetani et al., 2012). Thus, it is necessary to correct the volatile concentrations of melt inclusions to obtain the original concentration in the trapped melt, and a range of experimental and numerical methods have been used to do this. These include reversing changes that occurred during cooling experimentally by re-heating the melt inclusion and using a combination of microanalytical techniques, numerical modeling, and mass balance calculations to reconstruct the bulk composition of the trapped melt.

In the experimental approach, melt inclusions are heated and homogenized (dissolution of all solid and volatile phases to produce a homogeneous melt/glass, in ideal cases) under controlled temperature, pressure, and oxygen fugacity. This may include optical monitoring of the melt inclusion during heating on a microscope-mounted heating stage, heating in a tube furnace at one atmosphere, or heating in either a cold-seal or internally-heated pressure vessel (Student and Bodnar, 1999). While experimental homogenization works well for inclusions trapped at temperatures less than ~1000 °C and hosted in quartz (Bodnar and Student, 2006), melt inclusions trapped at higher temperatures and hosted in olivine and some other phases are often problematic – especially for inclusions that are relatively H_2O-rich (see Esposito et al., 2012). It has been shown that melt inclusions lose more H_2O during longer heating experiments (Massare et al., 2002; Severs et al., 2007; Bucholz et al., 2013). The change in density of the melt resulting from H^+ diffusion causes depressurization to occur, promotes the formation of shrinkage bubbles, and results in a homogenization temperature that exceeds the original trapping temperature (Danyushevsky et al., 2002). Thus, a consequence of H^+ diffusion is that H_2O-rich olivine-hosted melt inclusions often contain a bubble after 1 atm reheating experiments, and overheating the inclusion beyond the trapping temperature would compromise the composition of the inclusion by dissolving excess olivine into the melt. To solve this problem, Mironov et al. (2015) describe a method in which melt inclusions are heated in a pressure vessel in the presence of a hydrous glass under conditions similar to those presumed to be present when the melt inclusions were trapped (Mironov and Portnyagin, 2011). Because of the experimentally-generated water fugacity gradient, H_2O diffuses into the melt inclusions and rehydrates the melt to its original H_2O content, and samples are rapidly quenched (~150 °C/s) to prevent diffusive loss of H_2O following the experiment. As a result, CO_2 and other volatiles dissolve back into the melt at the temperature of trapping and do not require overheating.

As an alternative to the experimental approach, it is sometimes desirable to reconstruct the bulk compositions of melt inclusions without reheating them, such as when there is a need to avoid damaging a precious sample (e.g. Harvey and McSween, 1992; Goodrich et al., 2013), to preserve chemical gradients that record information about kinetically-limited processes (e.g. Newcombe et al., 2014), or because the equipment required for controlled heating experiments is unavailable. In these cases, the composition of the trapped melt can be reconstructed by determining the compositions and relative proportions of the various phases in the inclusion and estimating the bulk composition of the melt inclusion using a mass balance approach. Then, a numerical approach may be used to account for the effects of post-entrapment crystallization by incrementally adding host phase back into the melt until the calculated composition of the melt is in equilibrium with the host. This method works best with samples erupted as fine-grained tephras because H_2O loss is limited by the relatively rapid cooling (Lloyd et al., 2013) and inclusions that contain only glass ± vapor. It has been demonstrated in several recent studies that the CO_2 content of glassy, bubble-bearing melt inclusions can be determined based on Raman analysis (Esposito et al., 2011; Hartley et al., 2014; Moore et al., 2015; Aster et al., 2016) or cryometric analysis (Naumov et al., 2006) of the vapor bubble combined with other in situ microbeam analyses to determine the major, trace, and volatile composition of the glass. Additionally, the composition and density of the fluid exsolved into the bubble over the cooling interval between trapping and eruption can be estimated by numerical modeling (e.g. Anderson and Brown, 1993; Wallace et al., 2015; Aster et al., 2016).

Because of the benefits listed above, the approach of using mass-balance calculations to restore the CO_2 contents of unheated melt inclusions erupted in tephras is gaining acceptance, but there are a few notable disadvantages associated with this approach. For example, uncertainties incurred by mass-balance calculations associated with the method are not well understood. Previous studies have reported that minerals containing C, H, S, F, and Cl commonly form at the glass-vapor interface in melt inclusions (e.g. Kamenetsky et al., 2002; Esposito et al., 2016), but these minerals are rarely considered in studies to determine the composition of the vapor phase and/or the volatile content of melt inclusions (Kamenetsky et al., 2007; Moore et al., 2015; Esposito et al., 2016). Additionally, restricting sampling to fresh tephras and lavas with rapidly-quenched inclusions limits the availability, quality, and representativeness of sample material. For these reasons, it is useful to compare the compositions of unheated melt inclusions to inclusions that have been experimentally treated, but there are few studies have directly compared results from the Raman mass-balance approach with compositions determined after experimental homogenization (e.g. Wallace et al., 2015). To explore the relative merits of both approaches, we used Raman analyses and a mass balance approach following the methods described by Moore et al. (2015) to analyze melt inclusions from a suite of samples from the Klyuchevskoy volcano (Kamchatka). Previous studies (Mironov and Portnyagin, 2011; Mironov et al., 2015) determined the compositions of these same and similar melt inclusions after experimentally rehydrating and homogenizing the inclusions. We also use the method described by Wallace et al. (2015) to numerically estimate the amount of CO_2 exsolved into the bubbles.

2. Sample description

The melt inclusions analyzed in this study are hosted by olivine (Fo > 84) from lava and tephra samples from the eruption that formed the ~3 ka Bulochka cinder cone (V. Ponomavera, personal communication) on the flank of Klyuchevskoy volcano in the Kamchatka arc. The inclusions in this study are separated into three groups according to their host lithology and method of study: 1) unheated (as found) inclusions in olivines that had been separated from tephra samples, 2) recrystallized melt inclusions in olivine from a lava flow that were heated at 1 atm under dry conditions (Mironov and Portnyagin, 2011), and 3) inclusions from the same lava flow that were heated at ≥300 MPa in the presence of a hydrous glass (Mironov et al., 2015). Hereafter, these samples are referred to as *unheated*, *dry reheated*, and *experimentally rehydrated*, respectively. The proportion of CO_2 contained in the bubble was determined for all three groups using Raman spectroscopy. We present new analyses of the inclusion glass in the unheated group only; previously reported glass compositions are used for dry reheated and experimentally rehydrated groups (Mironov and Portnyagin, 2011 and Mironov et al., 2015 respectively).

Melt inclusions from the *unheated* tephra samples were prepared by polishing olivine crystals to expose the glass without breaching the bubble, as described by Moore et al. (2015). The splitting of the Fermi diad (Δ, cm^{-1}) could be quantified in approximately 95% of the inclusions analyzed. Vapor bubbles were analyzed by Raman spectroscopy in the

Fluids Research Laboratory at Virginia Tech. The major element composition of the glass was determined by electron probe microanalysis in the Electron Beam Laboratory at Virginia Tech. The host olivines in the unheated group have a mean composition of Fo 86.2 and a range of 84.6 to 87.5, which is less primitive than olivines analyzed by Mironov and Portnyagin (2011) and Mironov et al. (2015). The volatile composition of the glass was determined by secondary ion mass spectrometry (SIMS) using the Cameca 1280 ion microprobe at the Woods Hole Oceanographic Institute and the glass standards and calibration protocol described by Shimizu et al. (2009). The program *Petrolog3* (Danyushevsky and Plechov, 2011) was used to apply a correction to the unheated inclusions for Fe-loss and PEC. CO_2 concentrations reconstructed to include CO_2 in the bubble were determined using mass balance calculations as described in Moore et al. (2015).

The major element and volatile composition of the glass phase in *dry reheated* melt inclusions are reported by Mironov and Portnyagin (2011). The studied olivines (Fo 88.5–90.6) were collected from lavas and contain only recrystallized melt inclusions; glassy inclusions that could be analyzed "as found" without reheating were not present. Melt inclusions in olivines from these samples were heated at 1 atm (as described by Mironov and Portnyagin, 2011) and contain bubbles after reheating above 1300 °C. Unfortunately, the melt inclusions from the original dry reheated group described by Mironov and Portnyagin (2011) were subsequently analyzed by laser ablation and destroyed. The dry reheated inclusions analyzed by Raman in this study are not the same inclusions for which glass compositions are available from Mironov and Portnyagin (2011), nonetheless they are from the same sample suite and had also been previously reheated as described in that study. The splitting of the Fermi diad (Δ, cm^{-1}) could be quantified in approximately 70% of the inclusions analyzed, and the lower proportion of CO_2 quantification may be because the inclusions were in an epoxy multi-grain mount that was not specifically prepared to minimize the depth of the bubbles below the surface.

Major element, volatile contents and host olivine (Fo 85.3–90.9) compositions of the *experimentally rehydrated* melt inclusions are reported by Mironov et al. (2015). Some of the inclusions contain small bubbles because the melt inclusions were variably rehydrated, and we analyzed these using Raman spectroscopy. The experimentally rehydrated melt inclusions were not analyzed (destroyed) using laser ablation and, as a result, we were able to analyze the same inclusions described by Mironov et al. (2015). The amount of CO_2 in the bubble could be quantified in fewer than half of these inclusions.

A full description of the analytical methods and tables containing melt inclusion compositions used in this study can be found in the Supplementary material.

3. Results and discussion

3.1. Volatiles contained in the bubble

In general, bubbles in the dry reheated inclusions are the largest (~4–10 vol%), bubbles in the experimentally rehydrated inclusions are the smallest (~0–2 vol%), and bubbles in the unheated melt inclusions are of intermediate size (~2–5 vol%). The relative uncertainty of the bubble volume is approximately 50% (2σ) based on repeated measurements of the relative bubble volume. For unheated melt inclusions with vapor bubbles occupying 2–5 vol% of the inclusion, we assume an absolute uncertainty of ±2 vol% to account for both the uncertainty

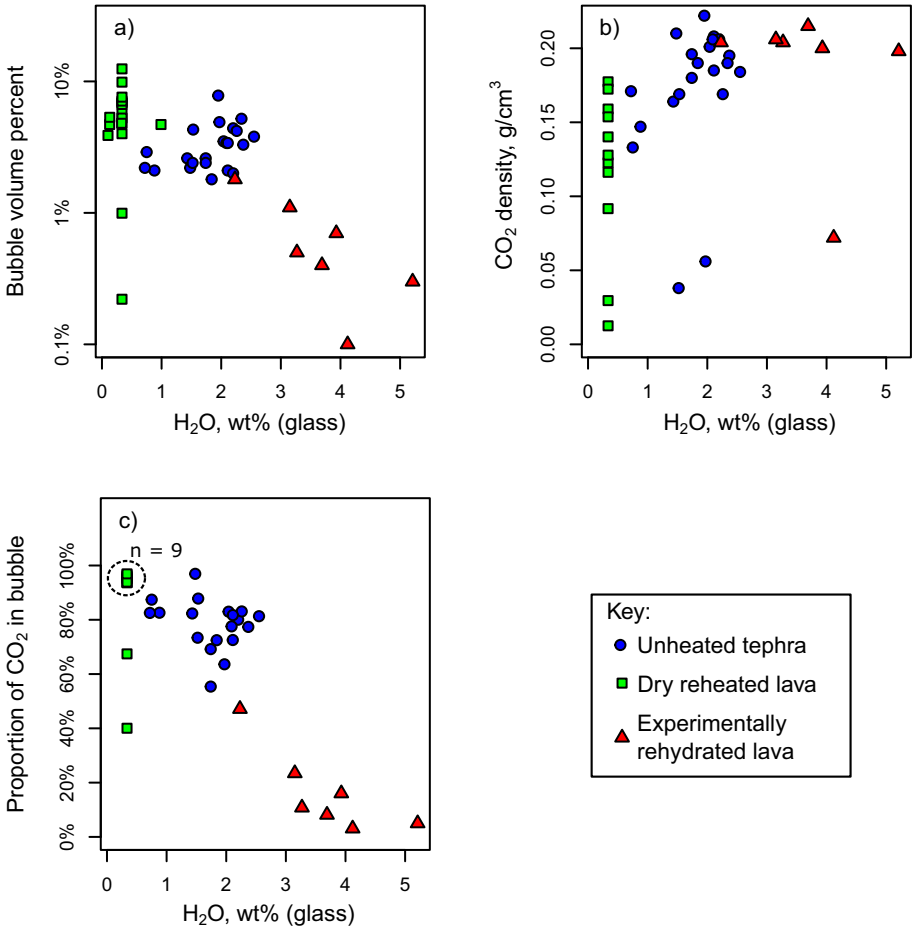

Fig. 1. Bubble volume (a), CO_2 fluid density (b), and proportion of total CO_2 in the melt inclusion that is contained in the bubbles (c), plotted as a function of the H_2O concentration in the glass. For *dry reheated* inclusions, average glass compositions from Mironov and Portnyagin (2011) were used because inclusion glasses were not analyzed in this study.

associated with measuring the dimensions of the inclusion petrographically and the additional uncertainty associated with assuming the unknown third dimension of the inclusion. In some cases, it is reasonable to assume that bubbles larger than about 5 vol% of the inclusion represent inclusions that have partially decrepitated, trapped a separate vapor phase along with the melt or, alternatively, that the melt inclusion and/or vapor bubble is relatively "flat" (tabular) in shape such that the relationship between the relative area of the bubble and the volume proportion observed under the microscope is different than if the bubble were spherical. For example, a given vapor bubble to total inclusion area that corresponds to 2 vol% if the bubble and inclusion are both spherical corresponds to 7.4 area percent if the inclusion and bubble are flat (i.e., circles with no third dimension). However, because we did not observe any flattened melt inclusions (i.e. as viewed from the side), and because the bubbles in the dry reheated inclusions are systematically larger than bubbles from the other two groups (Fig. 1a), the larger volume fraction of vapor for the inclusions is more likely a result of the nearly complete H_2O loss from the inclusions during their slow cooling in a lava flow and subsequent reheating (Portnyagin et al., 2008; Mironov and Portnyagin, 2011).

The highest CO_2 density is found in bubbles in the experimentally rehydrated inclusions (about 0.2–0.25 g/cm^3), the dry reheated samples tend to have lowest density (about 0.01–0.15 g/cm^3), and the unheated melt inclusions have an intermediate CO_2 density (about 0.1–0.2 g/cm^3). The uncertainty of the CO_2 density is approximately ± 0.02 g/cm^3 (2σ) based on replicate analyses, but this value depends on the optical quality of each sample. Most of the CO_2 densities cluster near or just below the maximum possible density (0.21 g/cm^3) for pure CO_2 vapor at room temperature (Fig. 1b).

While the volatile component most often (and easily) detected in the vapor bubbles is CO_2, other volatile components were also recognized. During petrographic examination of the melt inclusions, we often observed small solid phases present at the bubble-glass interface (Fig. 2b). Crystals at the bubble-glass interface are often not recognized during normal transmitted light petrography (Fig. 2a) and are more easily recognized during petrographic examination in reflected light and/or with cross-polarized light (Fig. 2b). We attempted to identify the solid phases using Raman spectroscopy by focusing the laser beam on areas that are visibly covered by crystals and comparing the Raman spectra to known mineral spectra in the RRUFF mineral database (Lafuente et al., 2015). We analyzed the solids at the bubble-glass interface in 15 of the unheated melt inclusions. In three inclusions, a carbonate mineral (likely magnesite) was identified, and in 14 of the bubbles native S, sulfides, and/or sulfates were detected. Fig. 2c shows Raman spectra of two melt inclusions in which C- and S-bearing phases were identified. We note that this method of mineral identification provides results that are inconclusive, but our results are consistent with previous observations of daughter minerals in melt inclusions (e.g. Kamenetsky et al., 2002; Esposito et al., 2016). It is not possible to precisely determine the portion of the C and S in the melt inclusions that is contained within crystals that formed at the bubble-glass interface because these crystals have dimensions that approach the limit of optical resolution (≤500 nm).

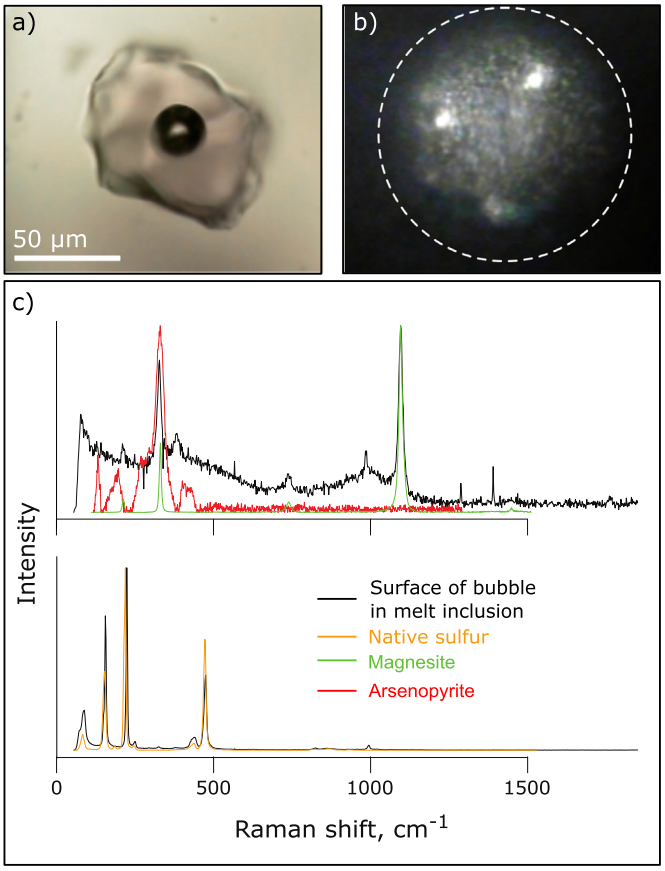

Fig. 2. Detection and identification of daughter crystals in unheated melt inclusions. a) A representative photomicrograph of an unheated melt inclusion from this study. b) Photomicrograph of a bubble contained in an unheated melt inclusion from this study. The dashed circle (diameter = 30 μm) indicates the outer edge of the bubble. Crystals at the edge of melt inclusion bubbles (on the "top" of the bubble in the photograph) are most easily recognized when viewed under reflected, cross-polarized light as shown. c) Raman spectra of daughter crystals at the bubble-glass interface in unheated melt inclusions. Spectra collected from melt inclusions are shown in black. Spectra of magnesite (green), arsenopyrite (red), and native sulfur (orange) from the RRUFF database (Lafuente et al., 2015) are shown for comparison.

3.2. Volatiles contained in the glass

After correcting for PEC, unheated melt inclusions are estimated to contain 54–862 ppm CO_2 (with an outlier at 1528 ppm) and up to ~2.5 wt% H_2O in the glass. The CO_2 content is significantly higher than that of the glass in melt inclusions from dry reheated lavas (84–300 ppm CO_2) reported by Mironov and Portnyagin (2011) and lower than the CO_2 content of the glass in unheated melt inclusions in tephras (979–1198 ppm CO_2) reported by Mironov et al. (2015). H_2O and CO_2 concentrations in the glass show a reasonably good correlation (Fig. 3a), which agrees with the conceptual framework described by Mironov et al. (2015) for interpreting compositions of melt inclusions that have experienced a combination of post-entrapment changes that result in depletion of both H_2O and CO_2 in the glass. According to this model, the CO_2 content of the melt (glass) decreases during post-entrapment crystallization owing to decompression within the inclusion and associated loss of CO_2 to the shrinkage bubble. Dehydration as a result of H^+ diffusion out of the melt inclusion causes the melt to lose both CO_2 and H_2O because CO_2 becomes less soluble and exsolves into the fluid bubble as H_2O is removed from the melt (Mironov and Portnyagin, 2011; Bucholz et al., 2013). These combined effects produce glass compositions that fall within a triangular region in H_2O-CO_2 space where the top corner of the shaded area shown in Fig. 3a represents a possible composition of the melt that was originally trapped.

3.3. Model-reconstruction of volatile contents

Previous studies have described a method to restore volatile contents of bubble-bearing melt inclusions using numerical modeling (Anderson and Brown, 1993; Wallace et al., 2015; Aster et al., 2016). In this study, we use this approach to provide an independent method for comparison with CO_2 contents obtained using Raman spectroscopy, but this method could be used in other cases to quantify the amount of CO_2 exsolved into bubbles when Raman spectroscopy is unavailable. Therefore, to evaluate this method as a potential alternative for the

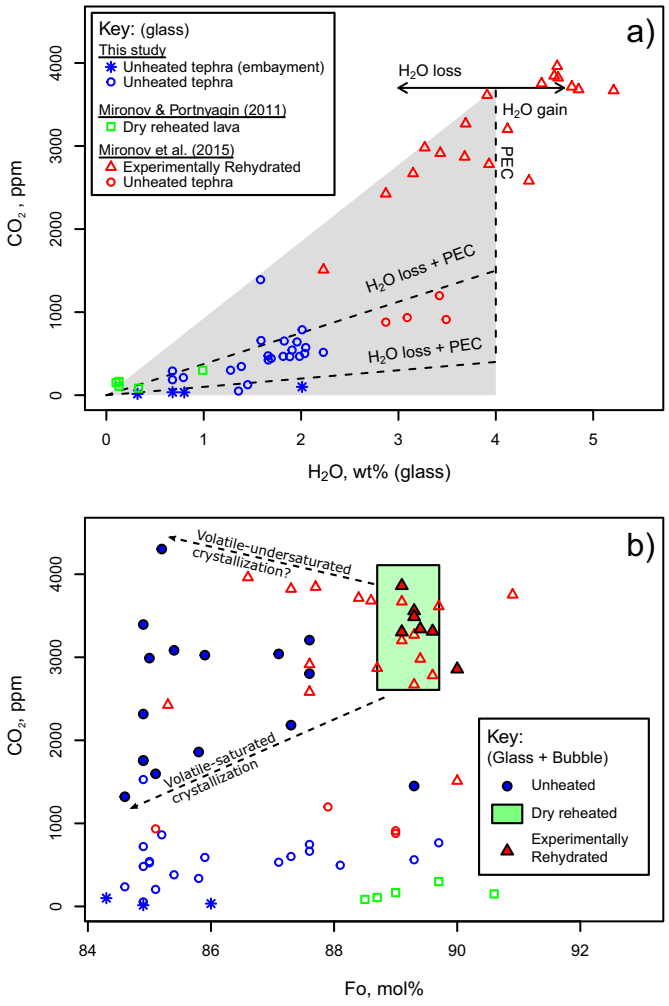

Fig. 3. a) H_2O vs CO_2 concentrations of glass in unheated, dry reheated, and experimentally rehydrated melt inclusions and embayments. Arrows qualitatively indicate the direction of compositional change associated with H_2O loss and H_2O gain. The shaded region and black dashed lines show the glass compositions that would be produced after trapping a melt with 4 wt% H_2O and 3800 ppm CO_2 after a combination of post-entrapment crystallization (PEC) and H_2O loss, and CO_2 exsolution into the bubble as described by Mironov et al. (2015). b) Forsterite vs CO_2 concentrations of glass in unheated, dry reheated, and experimentally rehydrated melt inclusions and embayments. The shaded green box indicates the interquartile range of dry reheated melt inclusion and host forsterite compositions, which were not analyzed for the same inclusion-host pairs.

Raman-mass balance method or experimental rehydration, we used a numerical approach adapted from Wallace et al. (2015) to calculate the volatile content of the bubbles in the unheated melt inclusions that were analyzed using Raman spectroscopy.

The inputs for the modeling approach are 1) the major and volatile element composition of the glass, 2) the composition of the host olivine (Fo #), and 3) the whole rock total FeO content of the tephra (Mironov et al., 2015). The program Petrolog3 was used to calculate the temperature interval over which PEC occurred and to calculate the composition of the melt before PEC. We used the olivine-melt model of Ford et al. (1983) and a NNO redox buffer for the PEC calculations. The melt-volatile solubility model of Iacono-Marziano et al. (2012) was used to determine the inclusion pressure and composition of the exsolving fluid at the end of PEC. This is assumed to represent the conditions when diffusion of volatiles into the bubble ceased. We used the empirically calibrated equation of state (EOS) of Duan and Zhang (2006) to calculate the molar volume of the mixed H_2O-CO_2 fluid. Molar volume and expansivity data for major element oxides (Lange and Carmichael, 1990; Lange, 1997) and experimentally-determined olivine expansivity data (Bouhifd et al., 1996) were used to calculate the differential volume change of the melt and olivine, respectively, over the PEC temperature interval (i.e. the volume of the exsolved fluid at the end of the cooling interval over which PEC occurs). Finally, the fluid composition, molar volume, and melt/host volume change were used to calculate the amount of CO_2 in the bubble.

The uncertainty associated with this numerical model was estimated by propagating the analytical uncertainty of the melt inclusion glass, host, and bulk rock compositions using a "Monte Carlo" approach. This yielded a propagated uncertainty of ~130 ppm, although this should be considered an underestimate because it does not account for other sources of uncertainty (e.g. experimentally-determined molar volumes, melt-volatile solubility relationships, or other factors such as the rate of CO_2 diffusion in the melt as conditions approach the glass transition).

To evaluate the model results, we compared the amount of CO_2 calculated for each inclusion using the Raman method to the same value calculated using the numerical method while ignoring the concentration of CO_2 measured in the glass (i.e. comparing the contribution of CO_2 from the bubbles only) – this was done to avoid introducing an autocorrelation effect. While the correlation between the calculated and observed CO_2 contents is low ($R^2 = 0.1$), the calculated CO_2 contents are within the analytical uncertainty of those determined by Raman spectroscopy in 14 out of 20 cases (Fig. 4). This is based on the assumption that the uncertainty of the Raman method is approximately ± 0.1 wt%, and this propagated uncertainty can be mostly attributed to errors associated with determining bubble volumes petrographically. These results suggest that the numerical approach may be used to provide a reasonable estimate of the amount of CO_2 in melt inclusion fluid bubbles if Raman analysis or experimental heating are unavailable. However, 17 of the 20 melt inclusions have calculated CO_2 contents that are lower than the CO_2 content determined using the Raman method, and this may indicate that the model does not account for a significant amount of CO_2 exsolution to the bubble that occurs during quenching. Because the uncertainty associated with petrographically-determined bubble volumes is a factor that limits our ability to evaluate the model results, we recommend that this uncertainty could be minimized either by 1) rotating the host crystals during polishing so that

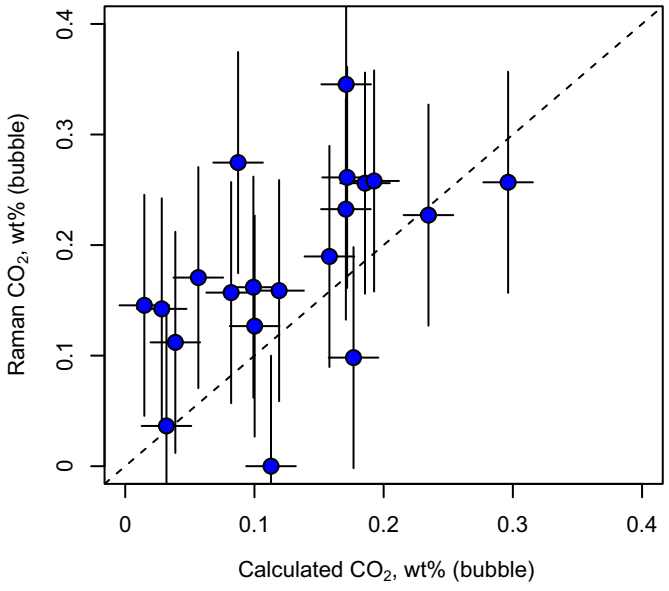

Fig. 4. Total CO_2 contents of unheated melt inclusions restored using both Raman spectroscopy and numerical modeling (calculated). Vertical error bars (2σ) represent combined uncertainty from petrographic determination of bubble volumes (±2 vol%) and CO_2 fluid density from Raman spectroscopy (±0.025 g/cm^3). Horizontal error bars indicate propagated uncertainties from model inputs including melt inclusion glass, host, and bulk rock compositions.

the inclusions can be viewed from two orthogonal angles to estimate the third dimension, or 2) by using X-ray microtomography (e.g. Gaetani et al., 2017) do determine the volume proportions of bubble-bearing inclusions more precisely, or 3) by using the spindle stage to observe the MI from various orientations (Anderson and Bodnar, 1993).

4. Discussion

When the melt inclusion compositions are restored to include CO_2 in the bubble, the CO_2 contents of all three groups of samples have maximum CO_2 contents that are approximately 0.4 wt% (Fig. 5) which is close to the CO_2 content of completely homogenized inclusions reported by Mironov et al. (2015). In the unheated inclusions, 50–90% of CO_2 is contained in the bubble. In the dry reheated melt inclusions, about 90% of the CO_2 is contained in the bubble assuming an average concentration of 162 ppm CO_2 in the glass as reported by Mironov and Portnyagin (2011); this assumption has a negligible impact on the total CO_2 concentration calculated for the inclusions because the CO_2 concentrations in the glass do not exceed 300 ppm for any of the dry reheated inclusions. In the experimentally rehydrated melt inclusions, 10–20% of the CO_2 is contained in the bubble for those inclusions in which the bubbles have not been completely redissolved into the melt during homogenization. The volumes, densities, and thus the proportion of CO_2 in the melt inclusions contained in the bubble are correlated with the H_2O concentration in the glass (Fig. 1), which also supports the hypothesis that the amount of CO_2 remaining in the glass is controlled by H^+ diffusion.

Although the maximum CO_2 contents of unheated, dry reheated and experimentally rehydrated melt inclusions are similar, many of the unheated inclusions contain significantly less CO_2 than the experimentally rehydrated inclusions, even after the CO_2 in the bubble has been added to the glass. This discrepancy may reflect either a post-entrapment process involving formation of carbonates at the bubble-glass interface (thus sequestering some of the CO_2 as carbonate) or a pre-entrapment effect like degassing of the melt between the time when the experimentally rehydrated and unheated melt inclusions were trapped.

To evaluate the possibility that CO_2 in the unheated melt inclusions was sequestered by carbonates, we systematically analyzed the surface of each bubble using Raman spectroscopy. Carbonates were only detected in ~20% of the inclusions analyzed, and there was no observed correlation between the presence of a carbonate peak and the calculated CO_2 content. Furthermore, if carbonate daughter crystals were pervasive in the unheated melt inclusions, then we would expect that the amount of CO_2 calculated by the numerical model would be significantly higher than the CO_2 content determined from Raman analysis, but this was not the case. For these reasons, it is unlikely that the lower CO_2 contents observed in the unheated melt inclusions can be attributed solely to formation of carbonate daughter crystals.

Alternatively, it is possible that the unheated melt inclusions could have been trapped after a significant amount of degassing had occurred. The olivine host compositions of the experimentally rehydrated and dry reheated lava samples are slightly more primitive than the unheated tephra samples (Fig. 3b). This suggests that a small amount of crystallization and degassing could have occurred before the unheated melt inclusions were trapped (as discussed by Mironov and Portnyagin, 2011). Unfortunately, to evaluate this possibility more fully, it would be necessary to compare the relationships of other volatile components, which

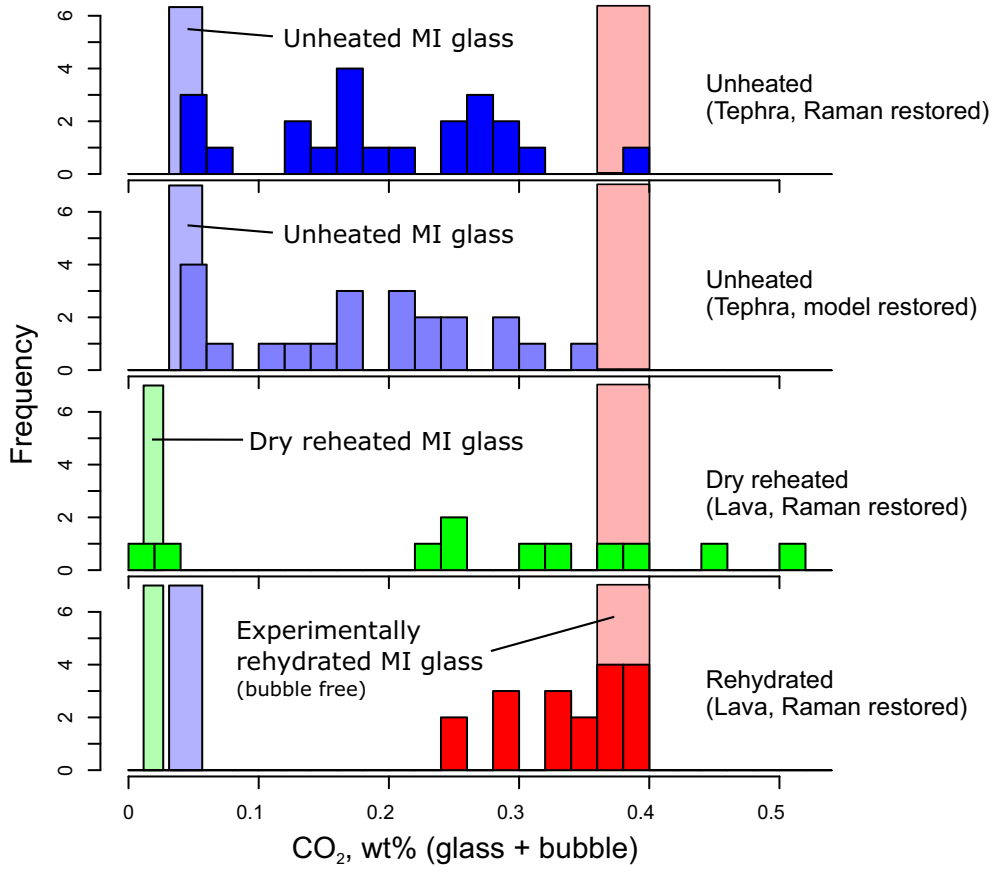

Fig. 5. Comparison of CO_2 contents in the glass and CO_2 contents restored using experimental and mass balance methods. Blue and green shaded bars in the background show typical values for CO_2 concentrations in melt inclusion glasses for dry reheated and unheated melt inclusions (interquartile range). Red shaded bars in the background show the range of CO_2 concentrations in bubble-free experimentally-rehydrated melt inclusions reported by Mironov et al. (2015).

Table 1
Advantages and disadvantages of the various sampling, analytical, and experimental methods used to estimate melt inclusion volatile budgets.

Method	Advantages	Disadvantages
Unheated melt inclusions: Identify glassy melt inclusions and analyze "as found"	• Requires minimal sample preparation. • No experimental apparatus or significant experimental expertise is required. • Inclusions are less likely to experience post-entrapment processes and will therefore preserve the original melt composition. • Preserves chemical gradients that provide information about diffusion kinetics	• Requires samples of fresh tephras or lavas with rapidly--quenched inclusions, and may limit the availability of sample material. • Large uncertainties may be associated with CO_2 contents restored using mass balance calculations. • Daughter minerals at the bubble-glass interface may sequester a significant portion of the volatile elements that must be accounted for.
Dry reheated melt inclusions: Identify glassy or recrystallized melt inclusions, reheat at ambient pressure, and analyze	• If, following reheating, the inclusion contains only glass (no crystals or bubbles), initial CO_2 (as well as S and Cl) content of the homogenized inclusion can be determined with high precision using SIMS or FTIR analysis of the glass. • Potentially re-dissolves any carbonates or sulfur-bearing phases that may have formed at the bubble-glass interface back into the melt. • Requires less time and expertise, and does not require sophisticated equipment for high-pressure experiments.	• Requires a one-atmosphere furnace to heat the inclusions and a sealed environment to limit sample oxidation. • Original H_2O contents and chemical gradients that provide information about diffusion kinetics may not be preserved. • Large uncertainties may be associated with CO_2 contents restored using mass balance calculations if a bubble remains after quenching. • Sample material may be damaged or destroyed during the reheating and quenching process. • Significantly dehydrated inclusions usually fail to homogenize.
Experimentally rehydrated melt inclusions: Identify glassy or recrystallized melt inclusions, reheat under controlled P-T-f_{O2}-a_{H2O}, and analyze	• If, following rehydration, the inclusion contains only glass (no crystals or bubbles), the volatile content of the homogenized inclusion can be determined with high precision using SIMS or FTIR analysis of the glass. • Can be applied to either glassy or partially crystallized MI. • Can be applied to homogenize completely dehydrated inclusions. • Potentially re-dissolves any carbonates or sulfur-bearing phases that may have formed at the bubble-glass interface back into the melt.	• Requires access to a high temperature, high pressure experimental laboratory to conduct rehydration experiments. • To achieve complete homogenization, requires independent estimate of potential P-T-f_{O2}-a_{H2O} conditions of melt inclusion entrapment, or multiple experiments at variable conditions may be required. • Original H_2O contents and chemical gradients that provide information about diffusion kinetics may not be preserved. • Sample material may be damaged or destroyed during the reheating and quenching process.

in this case have been compromised by H_2O loss and the formation of S-bearing (and potentially Cl-bearing) daughter crystals.

5. Summary and recommendations

Three different methods have been tested to reconstruct the volatile contents of melt inclusions in olivine from the Klyuchevskoy volcano, including analysis of (1) unheated (as found) inclusions in olivines from tephra samples (referred to as *unheated MI*), 2) inclusions in olivine from a lava flow that were heated at 1 atm under dry conditions (referred to as *dry reheated MI*), and 3) inclusions from the same lava flow that were heated at ≥300 MPa in the presence of a hydrous glass (referred to as *experimentally rehydrated MI*). In the case of this study, our results indicate that all three methods are effective for determining the original CO_2 contents of bubble-bearing melt inclusions, but there are clear advantages and disadvantages associated with each of these approaches (listed in Table 1). Because of these differences, we suggest that a robust melt inclusion dataset will include both melt inclusions that have been analyzed "as found" and melt inclusions that have undergone experimental treatment. Uncertainties associated with mass balance calculations are particularly problematic, and further work will be necessary to increase the precision with which the relative proportions and glass and fluid can be determined. For example, Gaetani et al. (2017) recently demonstrated that it is possible to precisely determine the volumes of the vapor bubble and the glass using X-ray microtomography. This approach is promising and should be adopted when possible. The presence of volatile-bearing daughter minerals is also problematic: even in cases where melt inclusions are quenched quickly, carbonates and other daughter minerals that form on the surface of the bubble may alter the volatile element distribution within the inclusion. It is likely that reheating inclusions (dry reheating or rehydration) will cause these daughter minerals to re-dissolve in the melt, but it is not clear 1) whether these daughter minerals may reform during or after quenching, and 2) whether other volatile elements may remain as a fluid phase after reheating (e.g. SO_2). Thus, we recommend additional studies to compare the volatile compositions of naturally quenched and reheated melt inclusions from rapidly cooled tephra samples to determine the stability limits of these daughter crystals and the kinetics of their formation during and after cooling. Finally, while numerical modeling may be a good alternative for in situ analysis of fluid bubbles, further sensitivity analysis and validation of the model using melt inclusions with a greater range of compositions will be necessary to improve this approach.

Acknowledgements

This work was supported by NSF grants EAR-1802012, EAR-1249412, and OCE-1756349 to EG and 1624589 to RJB. A contribution from the Vernadsky Institute core funding to NM and MP (theme AAAA-A16-116030110015-7) is kindly acknowledged. Charles Farley provided technical assistance with Raman analyses. Brian Monteleone and Nobu Shimizu provided technical assistance with SIMS analyses. Luca Fedele and Robert Tracy provided technical assistance with EPMA analyses. LM wishes to thank Jarek Trela for his help and support during SIMS and EPMA analyses. We thank Leonid Danyushevsky and an anonymous reviewer for their suggestions, which greatly improved the quality of this manuscript.

Appendix A. Supplementary data

Supplementary data to this article can be found online at https://doi.org/10.1016/j.jvolgeores.2018.03.007.

References

Anderson, A.J., Bodnar, R.J., 1993. An adaptation of the spindle stage for geometric analysis of fluid inclusions. Am. Mineral. 78, 657–664.
Anderson, A.T., Brown, G.G., 1993. CO_2 contents and formation pressures of some Kilauean melt inclusions. Am. Mineral. 78, 794–803.
Aster, E.M., Wallace, P.J., Moore, L.R., Watkins, J., Gazel, E., Bodnar, R.J., 2016. Reconstructing CO_2 concentrations in basaltic melt inclusions using Raman analysis of vapor bubbles. J. Volcanol. Geotherm. Res. 323, 148–162.
Bodnar, R.J., Student, J.J., 2006. Melt inclusions in plutonic rocks: petrography andmicrothermometry. In: Webster, J.D. (Ed.), Melt Inclusions in Plutonic Rocks. Mineralogical Association of Canada, Short Course 36, pp. 1–26.
Bouhifd, M.A., Fiquet, A.G., Richet, P., 1996. Thermal expansion of forsterite up to the melting point. Geophys. Res. Lett. 23 (10), 1143–1146.

Bucholz, C.E., Gaetani, G.A., Behn, M.D., Shimizu, N., 2013. Post-entrapment modification of volatiles and oxygen fugacity in olivine-hosted melt inclusions. Earth Planet. Sci. Lett. 374, 145–155.
Burton, M.R., Sawyer, G.M., Granieri, D., 2013. Deep carbon emissions from volcanoes. Rev. Mineral. Geochem. 75, 323–354.
Chiodini, G., Cardellini, C., Amato, A., Boschi, E., Caliro, S., Frondini, F., Ventura, G., 2004. Carbon dioxide Earth degassing and seismogenesis in central and southern Italy. Geophys. Res. Lett. 31.
Danyushevsky, L.V., Plechov, P., 2011. Petrolog3: integrated software for modeling crystallization processes. Geochem. Geophys. Geosyst. 12, 7 (32 pp).
Danyushevsky, L.V., McNeill, A.W., Sobolev, A.V., 2002. Experimental and petrological studies of melt inclusions in phenocrysts from mantle-derived magmas: an overview of techniques, advantages and complications. Chem. Geol. 183, 5–24.
Dasgupta, R., 2013. Ingassing, storage, and outgassing of terrestrial carbon through geologic time. Rev. Mineral. Geochem. 75, 183–229.
Duan, Z.H., Zhang, Z.G., 2006. Equation of state of the H_2O-CO_2 system up to 10 GPa and 2573 K: molecular dynamics simulations with ab initio potential surface. Geochim. Cosmochim. Acta 70 (9), 2311–2324.
Esposito, R., Bodnar, R.J., Danyushevsky, L.V., de Vivo, B., Fedele, L., Hunter, J., Lima, A., Shimizu, N., 2011. Volatile evolution of magma associated with the Solchiaro eruption in the Phlegrean Volcanic District (Italy). J. Petrol. 52 (12), 2431–2460.
Esposito, R., Klebesz, R., Bartoli, M., Klukin, Y., Moncada, D., Doherty, A., Bodnar, R.J., 2012. Application of the Linkam TS1400XY heating stage to melt inclusion studies. Cent. Eur. J. Geosci 4 (2), 208–218.
Esposito, R., Lamadrid, H.M., Redi, D., Steele-MacInnis, M., Bodnar, R.J., Manning, C.E., De Vivo, B., Cannatelli, C., Lima, A., 2016. Detection of liquid H_2O in vapor bubbles in reheated melt inclusions: implications for magmatic fluid composition and volatile budgets of magmas? Am. Mineral. 101, 1691–1695.
Ford, C.E., Russell, D.G., Craven, J.A., Fisk, M.R., 1983. Olivine-liquid equilibria; temperature, pressure and composition dependence of the crystal/liquid cation partition coefficients for Mg, Fe2+, Ca and Mn. J. Petrol. 24, 256–265.
Gaetani, G., O'Leary, J., Shimizu, N., 2012. Post-entrapment changes to H_2O and CO_2 in olivine-hosted melt inclusions. Mineral. Mag. 75, 879.
Gaetani, G.A., Le Roux, V., Klein, F., Moore, L.R., Bodnar, R.J., Maclennan, J., 2017. X-ray microtomography-based reconstruction of total CO_2 in olivine-hosted melt inclusions. Goldschmidt 2017 Abstract.
Gazel, E., Plank, T., Forsyth, D.W., Bendersky, C., Lee, C-T.A., Hauri, E.H., 2012. Lithosphere versus asthenosphere mantle sources at the Big Pine Volcanic Field, California. Geochem. Geophys. Geosyst. 13, 1–25.
Goodrich, C.A., Treiman, A.H., Filiberto, J., Gross, J., Jercinovic, M., 2013. K2O-rich trapped melt in olivine in the Nakhla meteorite: implications for petrogenesis of nakhlites and evolution of the Martian mantle. Meteorit. Planet. Sci. 12, 2371–2405.
Hartley, M.E., Maclennan, J., Edmonds, M., Thordarson, T., 2014. Reconstructing the deep CO_2 degassing behavior of large basaltic fissure eruptions. Earth Planet. Sci. Lett. 393, 120–121.
Harvey, R.P., McSween, H.Y., 1992. The parent magma of the nakhlite meteorites: clues from melt inclusions. Earth Planet. Sci. Lett. 111, 467–482.
Iacono-Marziano, G., Morizet, Y., Le Trong, E., Gaillard, F., 2012. New experimental data and semi-empirical parameterization of H_2O–CO_2 solubility in mafic melts. Geochim. Cosmochim. Acta 97, 1–23.
Kamenetsky, V.S., Davidson, P., Mernagh, T.P., Crawford, A.J., Gemmell, J.B., Portnyagin, M.V., Shinjo, R., 2002. Fluid bubbles in melt inclusions and pillow-rim glasses: high-temperature precursors to hydrothermal fluids? Chem. Geol. 183, 349–364.
Kamenetsky, V.S., Pompilio, M., Metrich, N., Sobolev, A.V., Kuzmin, D.V., Thomas, R., 2007. Arrival of extremely volatile-rich high-Mg magmas changes explosivity of Mount Etna. Geology 35 (3), 255–258.
Lafuente, B., Downs, R.T., Yang, H., Stone, N., 2015. The power of databases: the RRUFF project. In: Armbruster, T., Danisi, R.M. (Eds.), Highlights in Mineralogical Crystallography. W. De Gruyter, Berlin, Germany, pp. 1–30.
Lange, R.A., 1997. A revised model for the density and thermal expansivity of K_2O-Na_2O-CaO-MgO-Al_2O_3-SiO_2-liquids from 700 to 1900 K: extension to crustal magmatic temperatures. Contrib. Mineral. Petrol. 130, 1–11.
Lange, R.A., Carmichael, I.S.E., 1990. Thermodynamic properties of silicate liquids with emphasis on density, thermal expansion, and compressibility. Rev. Mineral. 24, 25–59.
Lloyd, A.S., Plank, T., Ruprecht, P., Hauri, E.H., Rose, W., 2013. Volatile loss from melt inclusions in pyroclasts of differing sizes. Contrib. Mineral. Petrol. 165, 129–153 (published online, online 28 September 2012).
Massare, D., Metrich, N., Clocchiatti, R., 2002. High-temperature experiments on silicate melt inclusions in olivine at 1 atm: inference on temperatures of homogenization and H_2O concentrations. Chem. Geol. 183, 87–98.
Metrich, N., Wallace, P.J., 2008. Volatile abundances in basaltic magmas and their degassing paths tracked by melt inclusions. Rev. Mineral. Geochem. 69, 363–402.
Mironov, N.L., Portnyagin, M.V., 2011. H_2O and CO_2 in parental magmas of Kliuchevskoi volcano inferred from study of melt and fluid inclusions in olivine. Russ. Geol. Geophys. 52, 1353–1367.
Mironov, N., Portnyagin, M., Botcharnikov, R., Gurenko, A., Hornle, K., Holtz, F., 2015. Quantification of the CO_2 budget and H_2O–CO_2 systematics in subduction-zone magmas through the experimental hydration of melt inclusions in olivine at high H_2O pressure. Earth Planet. Sci. Lett. 425, 1–11.
Moore, L.R., Gazel, E., Tuohy, R., Lloyd, A.S., Esposito, R., Steele-MacInnis, M., Hauri, E.H., Wallace, P.J., Plank, T., Bodnar, R.J., 2015. Bubbles matter: an assessment of the contribution of vapor bubbles to melt inclusion volatile budgets. Am. Mineral. 100, 806–823.
Naumov, V.B., Portnyagin, M.V., Tolstykh, M.L., Yarmolyuk, V.V., 2006. Chemical composition and crystallization conditions of trachybasalts from the Dzhida Field, Southern Baikal volcanic area: evidence from melt and fluid inclusions. Geochem. Int. 44 (3), 286–295.
Newcombe, M.E., Fabbrizio, A., Zhang, Y., Ma, C., Le Voyer, M., Guan, Y., Eiler, J.M., Saal, A.E., Stolper, E.M., 2014. Chemical zonation in olivine-hosted melt inclusions. Contrib. Mineral. Petrol. 168, 1030.
Portnyagin, M.V., Hoernle, K., Plechov, P.Y., Mironov, N.L., Khubunaya, S.A., 2007. Constraints on mantle melting and composition and nature of slab components in volcanic arcs from volatiles (H_2O, S, Cl, F) and trace elements in melt inclusions from the Kamchatka Arc. Earth Planet. Sci. Lett. 255 (1–2), 53–69.
Portnyagin, M., Almeev, R., Matveev, S., Holtz, F., 2008. Experimental evidence for rapid water exchange between melt inclusions in olivine and host magma. Earth Planet. Sci. Lett. 272, 541–552.
Roedder, E., 1979. Origin and significance of magmatic inclusions. Bull. Mineral. 102, 467–510.
Roedder, E., 1984. Fluid inclusions. Mineralogical Society of America, Reviews in Mineralogy vol. 12 (644 pp).
Severs, M.J., Azbej, T., Thomas, J.B., Mandeville, C.W., Bodnar, R.J., 2007. Experimental determination of H_2O loss from melt inclusions during laboratory heating: evidence from Raman spectroscopy. Chem. Geol. 237, 358–371.
Shimizu, K., Shimizu, N., Komiya, T., Suzuki, K., Maruyama, S., Tatsumi, Y., 2009. CO_2-rich komatiitic melt inclusions in Cr-spinels within beach sand from Gorgona Island, Colombia. Earth Planet. Sci. Lett. 288, 33–43.
Sobolev, A.V., Danyushevsky, L.V., 1994. Petrology and geochemistry of boninites from the north termination of the Tonga Trench: constraints on the generation conditions of primary high-Ca boninite magmas. J. Petrol. 35, 1183–1211.
Student, J.J., Bodnar, R.J., 1999. Synthetic fluid inclusions XIV: coexisting silicate melt and aqueous fluid inclusions in the haplogranite–H_2O–NaCl–KCl system. J. Petrol. 40 (10), 1509–1525.
Wallace, P.J., 2005. Volatiles in subduction zone magmas: concentrations and fluxes based on melt inclusion and volcanic gas data. J. Volcanol. Geotherm. Res. 140, 217–240.
Wallace, P.J., Kamenetsky, V.S., Cervantes, P., 2015. Melt inclusion CO_2 contents, pressures of olivine crystallization, and the problem of shrinkage bubbles. Am. Mineral. 100, 787–794.